HHS Public Access

Author manuscript

Nat Immunol. Author manuscript; available in PMC 2009 May 01.

Published in final edited form as:

Nat Immunol. 2008 November ; 9(11): 1307–1315. doi:10.1038/ni.1662.

The actin regulator coronin-1A is mutated in a thymic egress deficient mouse strain and in a $T^{-}B^{+}NK^{+}$ SCID patient

Lawrence R. Shiow[1,2,3], **David W. Roadcap**[5], **Kenneth Paris**[7], **Susan R. Watson**[2], **Irina L. Grigorova**[1,2], **Tonya Lebet**[2,4], **Jinping An**[1,2], **Ying Xu**[1,2], **Craig N. Jenne**[1,2], **Niko Föger**[8], **Ricardo U. Sorensen**[7], **Christopher C. Goodnow**[6], **James E. Bear**[5], **Jennifer M. Puck**[3,4], and **Jason G. Cyster**[1,2,3]

[1] Howard Hughes Medical Institute, University of California San Francisco, San Francisco, CA

[2] Department of Microbiology and Immunology, University of California San Francisco, San Francisco, CA

[3] Biomedical Sciences Graduate Program, University of California San Francisco, San Francisco, CA

[4] Department of Pediatrics and Institute for Human Genetics, University of California San Francisco, San Francisco, CA

[5] Lineberger Comprehensive Cancer Center and Department of Cell and Developmental Biology, School of Medicine, University of North Carolina at Chapel Hill, Chapel Hill, NC

[6] John Curtin School of Medical Research, The Australian National University, Canberra, Australia

[7] Department of Pediatrics, Louisiana State University Health Sciences Center and Children's Hospital, New Orleans, LA

[8] Department of Immunology and Cell Biology, Leibniz Center for Medicine and Biosciences, Borstel, Germany

Abstract

Mice carrying the recessive peripheral T cell deficiency (*Ptcd*) locus have a block in thymic egress but the mechanism responsible is undefined. Here we found that *Ptcd* T cells have an intrinsic migration defect, impaired lymphoid tissue trafficking and irregularly shaped protrusions. Characterization of the *Ptcd* locus revealed an E26K point mutation within the actin regulator coronin-1A (*Coro1a*) that enhanced its inhibition of the actin regulator Arp2/3 and resulted in its mislocalization from the leading edge of migrating T cells. Discovery of another *Coro1a* mutant during an *N*-ethyl-*N*-nitrosourea (ENU) mutagenesis screen for T cell lymphopenic mice prompted us to evaluate a T cell-deficient, B cell- and NK cell-sufficient ($T^{-}B^{+}NK^{+}$) severe combined immunodeficiency (SCID) patient, whom we found had mutations in both *CORO1A* alleles. These findings establish a role for coronin-1A in T cell egress, identify a surface of coronin involved in

Correspondence should be addressed to: J.G.C. (Jason.Cyster@ucsf.edu).

Arp2/3 regulation, and reveal actin regulation as a biological process defective in human and mouse SCID.

INTRODUCTION

Following development in the thymus, mature thymocytes upregulate sphingosine-1-phosphate receptor 1 ($S1P_1$) and exit into the circulation to populate the naive T cell compartment. $S1P_1$ and its ligand sphingosine-1-phosphate (S1P) are required for egress of mature thymocytes 1. FTY720, a small molecule immunosuppressant in clinical trials for treatment of autoimmune disease, inhibits egress by modulating $S1P_1$ function 1. Beyond the $S1P_1$ requirement, little is understood about how T cells migrate out of the thymus.

The Cataract Shionogi (CTS) strain was initially isolated in the 1960's from a closed colony of ICR mice for exhibiting cataracts and microphthalmia 2. The CTS strain was later established to have a thymic egress defect 3 after it failed to reject MHC-disparate skin grafts 4. The nature of this recessive defect, named peripheral T cell deficiency (Ptcd), and its role in thymic egress has been unclear.

Coronins are actin regulators found in all eukaryotes 5. In addition to binding F-actin, coronins associate with and inhibit the nucleation-promoting Arp2/3 complex. Seven coronin family members exist in mammals, including coronin-1A (Coro1A), which is predominantly expressed in hematopoeitic cells. Coro1A-deficient mice have reduced peripheral T cells due to increased apoptosis 6,7 and in one study this was attributed to an excessive accumulation of F-actin 6. T cell migration was also reported to be defective 6,7, but this has been called into question 8. The latter authors also question whether Coro1A deficiency alters F-actin dynamics, and instead link the increased apoptosis to a T cell receptor (TCR) signaling defect 8. These conflicting reports with *Coro1a*-null mice have complicated the understanding of this actin regulator's role in T cell biology.

Here, we report that *Ptcd* T cells have an intrinsic migration defect that impairs thymic egress and trafficking through lymph nodes. We narrowed the *Ptcd* locus and identified a point mutation within Coro1A that causes mislocalization of the protein in T cells and increases its inhibition of Arp2/3 in biochemical assays. In a parallel effort to identify further trafficking mutants by screening mice carrying ENU-induced mutations for altered peripheral T cell numbers, we identified a strain that has 10-fold reduced Coro1A abundance and shows a similar phenotype to *Coro1a* 'knockout' mice. Comparison of *Ptcd* and Coro1A-deficient T cells allowed us to separate the defect in TCR-induced Ca^{++} signaling from the reduction in thymocyte surival. In addition to yielding new alleles of *Coro1a*, our mouse forward genetic approach led us to identify a $T^{-}B^{+}NK^{+}$ SCID patient with CORO1A deficiency.

RESULTS

Ptcd is an intrinsic T cell migration defect

To characterize the cellular basis for the *Ptcd* defect, we first backcrossed the *Ptcd* locus onto the C57BL/6 (B6) strain and confirmed the accumulation of mature single-positive

(SP) thymocytes ($CD69^{lo}$ $CD62L^{hi}$) and associated decrease in peripheral T cells (Fig. 1a and Supplementary Fig. 1 online). Irradiated wild-type mice that had been reconstituted with *Ptcd* bone marrow cells also had an accumulation of mature thymocytes and low circulating T cells (Fig. 1b) whereas reciprocal bone marrow chimeras did not exhibit such defects (Supplementary Fig. 2 online). These results localized the *Ptcd* defect to a hematopoeitic-derived cell and implicated impaired thymic egress of mature thymocytes as a pathogenic mechanism.

While normal amounts of $S1P_1$ were expressed on *Ptcd* mature SP thymocytes (Fig. 1c), $S1P_1$ function was impaired. In transwell migration assays, *Ptcd* mature CD4SP thymocytes were less efficient at migrating towards S1P than cells from control heterozygous littermates (Fig. 1d). The cells also migrated less efficiently to chemokines CCL21 and CXCL12. The response of *Ptcd* CD4 and CD8 double-positive (DP) thymocytes to CXCL12 was similarly reduced (Fig. 1e) and migration of *Ptcd* naïve splenic T cells was impaired while B cells migrated normally (Fig. 1f). Expression of CCR7 and CXCR4, the respective chemokine receptors that recognize CCL21 and CXCL12, were similar between *Ptcd* and control cells (Supplementary Fig. 3 online). These results indicate that T cells in *Ptcd* mice have a general, cell-intrinsic migration defect that impairs $S1P_1$ responsiveness and blocks thymic egress.

Ptcd T cells have entry, egress and motility defects

To test for peripheral trafficking defects, *Ptcd* and control T cells were co-transferred into wildtype recipients. At 1 h post-transfer, the ratio of *Ptcd*:control T cells was decreased in peripheral and mesenteric lymph nodes and increased in blood (Fig. 2a) indicating that *Ptcd* cells are less efficient at entering lymph nodes. Next, lymph node egress was tested using two approaches. First, *Ptcd* and control T cells were co-transferred at a 3:1 ratio to achieve equal proportions in the lymph nodes. At 24 h after transfer a significantly reduced proportion of *Ptcd* cells were found in lymph compared to lymph nodes (Fig. 2b) consistent with a reduced ability to exit into lymph. As an additional approach, we assessed the retention of *Ptcd* T cells within lymph nodes. After transfer of *Ptcd* and control T cells, entry into lymph nodes was blocked for 20 h with integrin-neutralizing antibodies. Roughly 60% of *Ptcd* T cells were retained in the lymph nodes compared with just 20% of control T cells (Fig. 2c). Together, these results demonstrate that *Ptcd* T cells are defective in exiting lymph nodes.

Two-photon microscopy on explanted lymph nodes from mice that had received fluorescently labeled cells showed that while control cells moved at median velocities of 9.5 microns/min, *Ptcd* cells moved at reduced median velocities of 6.6 microns/min (Fig. 2d and Supplementary Movie 1 online). In addition, *Ptcd* cells had increased turning angles (Fig. 2e), indicative of less directed paths and the cells failed to efficiently displace over time (Fig. 2f). These results demonstrate that in addition to blocking thymic egress, the *Ptcd* defect impairs trafficking through lymph nodes.

Coronin-1A is mutated at the *Ptcd* locus

The *Ptcd* locus was previously mapped to a 10.9 Mb region of chromosome 7 containing over 300 open reading frames 9. To refine the locus, we performed a mapping cross between CTS and B6, using the thymocyte accumulation to phenotype mice (Fig. 3a). We observed that the cataracts and microphthalmia were in F1 hybrids and failed to co-segregate with the recessive *Ptcd* trait (data not shown), consistent with an early report that these eye traits were autosomal dominant 10. After analyzing over 900 meiosis events, we further mapped the *Ptcd* locus to a 950 kb critical interval (Fig. 3b). This gene-rich interval contained 37 open reading frames including *Coro1a* (Fig. 3c). *Coro1a* was an attractive candidate gene for *Ptcd* because of its abundance in T cells 11 and the association of coronin family molecules with actin-based motility 5. Sequencing of *Ptcd* DNA revealed a G->A mutation in exon 2 of *Coro1a* (Fig. 3d), resulting in a non-conservative Glu->Lys substitution at residue 26 (E26K) in the beta-propeller domain (Fig. 3e). This residue is conserved in all annotated Coro1A sequences as well as charge conserved in a broad number of orthologs (Supplementary Fig. 4, online) and is in a surface exposed loop 12 adjacent to a region implicated in the close relative, Coro1B, as an actin binding site 13. Immunoblot analysis showed Coro1A abundance in total thymocytes did not vary between *Ptcd* and controls (Fig. 3f).

To exclude that mutations other than Coro1A^{E26K} may be responsible for the *Ptcd* phenotype, we tested for genetic complementation by crossing *Ptcd* with *Coro1a*$^{+/-}$ mice. As expected, the *Coro1a* wild-type allele complemented *Ptcd* defects in T cell lymphopenia and F-actin accumulation while the *Coro1a* null allele failed to complement (Supplementary Fig. 5a,b, online). In addition, mature thymocyte numbers in Ptcd/− mice were slightly elevated compared to Ptcd/+ (Supplementary Fig. 5c, online). While these studies do not exclude the possibility that the *Ptcd* interval contains additional genetic modifiers, the inability of the *Coro1a* null allele to rescue several of the *Ptcd* defects provides strong evidence that the Coro1A^{E26K} mutation results in the *Ptcd* phenotype.

ENU-mutant Koyaanisqatsi is a Coronin-1A hypomorph

In parallel to the above studies, we conducted an ENU mutagenesis screen to identify regulators of lymphocyte trafficking and egress. Koyaanisqatsi (*Koy*) was initially identified as a recessive mutant with a circulating T cell deficiency (Fig. 4a). Further characterization of *Koy* mice revealed a decrease both in mature thymocyte numbers and peripheral T cells (Fig. 4b and Supplementary Fig. 6). In transwell migration assays, *Koy* thymocytes and naive T cells migrated much less efficiently than littermate control cells (Fig. 4c). These findings in the *Koy* mice, along with an elevated phalloidin staining in *Koy* mature thymocytes (Fig. 4d), resembled those reported in *Coro1a*$^{-/-}$ mice generated by gene targeting 6. Upon sequencing *Koy* DNA, we identified an A->T substitution in exon 7 of *Coro1a* (Fig. 4e) resulting in an Asp->Val mutation at residue 278. This residue is located at a contact surface predicted to be critical for the proper assembly and stability of Coro1A 12, and immunoblot analysis of total thymocytes showed that *Koy* cells had roughly 10-fold reduced amounts of Coro1A (Fig. 4f). Taken together, these data indicate that *Koy* is a hypomorphic mutant of Coro1A.

Survival and Ca^{2+} flux in Coronin-1A mutants

A direct comparison of *Ptcd* with *Koy* and *Coro1a*$^{-/-}$ mice confirmed that the E26K mutation does not phenocopy the Coro1A deficient state. While *Ptcd* mutants have an accumulation of mature thymocytes (Fig. 1a), Coro1A-deficient mice have reduced numbers (Fig. 4b) due to reduced cell survival 6. Analysis of cell viability by loss of mitochondrial membrane potential (Fig. 5a) and annexin-V staining (Fig. 5b) revealed that mature thymocytes from *Ptcd* mice were comparable to wild-type controls whereas mature thymocytes from *Coro1a*$^{-/-}$ mice had reduced viability. However, *Ptcd* splenic T cells showed a similar defect in survival to *Coro1a*$^{-/-}$ cells (Fig. 5a,b).

A previous study has attributed the survival defect of *Coro1a*$^{-/-}$ T cells to downstream effects of excessive F-actin accumulation 6. Consistent with this interpretation, *Ptcd* mature thymocytes showed only a minor increase in F-actin as measured by phalloidin staining (Fig. 5c) whereas *Coro1a*$^{-/-}$ mature thymocytes and the similarly apoptosis prone *Ptcd* and *Coro1a*$^{-/-}$ splenic T cells all showed comparable two-fold elevations in phalloidin staining (Fig. 5c). However, the correlation between F-actin accumulation and reduced viability did not seem to hold for Ptcd/− T cells as they showed a similar elevation in phalloidin staining to *Coro1a*$^{-/-}$ T cells and yet were not reduced in number within the thymus (Supplementary Fig. 5). A recent study has suggested that the reduced viability of *Coro1a*$^{-/-}$ cells reflects a requirement for Coro1A in TCR-induced Ca^{2+} flux rather than in F-actin regulation 8. However, *Ptcd* and Coro1A-deficient mature CD4 SP thymocytes showed comparable Ca^{2+} flux defects following CD3 crosslinking (Fig. 5d). Furthermore, both *Ptcd* and Coro1A-deficient cells showed minimal defects in comparison to wild-type following co-crosslinking of CD3 and CD4, a treatment that may more closely mimic major histocompatibility complex class II-peptide engagement 14 (Fig. 5d). These findings dissociate the role of Coro1A in TCR-induced Ca^{2+} signaling from its role in thymocyte viability, but leave it unclear whether Coro1A acts via F-actin regulation or by some other mechanism to promote T cell survival.

Coro1A^{E26K} is mislocalized in *Ptcd* T cells

Coro1B regulates F-actin dynamics at the leading edge of migrating fibroblasts 15 and in migrating wild-type T cells, Coro1A was situated in F-actin– and Arp2/3-rich leading edge protrusions (Fig. 6a,b). The distribution of Coro1A^{E26K} in migrating *Ptcd* T cells was markedly altered and little of the protein could be detected at the leading edge (Fig. 6a), while Arp2/3 continued to concentrate in this region (Fig. 6b). Coro1A^{E26K} also similarly mislocalized when expressed in fibroblasts (Supplementary Fig. 7 online), indicating an intrinsic failure to distribute at the leading edge.

Real-time live cell imaging revealed that protrusions from migrating *Ptcd* T cells were irregularly shaped and often larger in size than protrusions in wild-type cells, consistent with a failure to properly regulate the actin cytoskeleton (Fig. 6c and Supplementary Movies 2–4 online). Similarly dysmorphic protrusions were observed with Ptcd/− compound mutant T cells (Supplementary Fig. 5d). The short *in vitro* survival of Coro1A-deficient T cells made assessments difficult, but these cells appeared more severely compromised in their migration than *Ptcd* T cells (Supplementary Movie 5 online). Together, these results establish that

Coro1A^{E26K} fails to distribute correctly in migrating T cells and the cells exhibit aberrant shape regulation.

E26K mutation in Coronin-1A enhances Arp2/3 inhibition

To understand the biochemical impact of the E26K mutation, we first looked at Coro1A's ability to bind F-actin. In co-sedimentation assays, Coro1A^{E26K} associated normally with F-actin (Fig. 6d). By contrast, Arp2/3 co-immunoprecipitated increased amounts of Coro1A^{E26K} from cell lysates relative to the wild-type protein (Fig. 6e). The corresponding mutation in Coro1B also resulted in an increased association with Arp2/3 (Supplementary Fig. 8 online). Consistent with increased interaction with Arp2/3, Coro1A^{E26K} was more efficient than wild-type Coro1A at inhibiting Arp2/3 activity in actin polymerization assays (Fig. 6f).

To examine how this biochemical gain-of-function mutation manifests as a recessive *Ptcd* allele, we analyzed T cells from Ptcd/+ and Ptcd/− mice. As expected, the Coro1A distribution in Ptcd/− T cells (Fig. 6g) was similar to Ptcd/Ptcd T cells (Fig. 6a). In Ptcd/+ T cells, Coro1A was present both at and mislocalized away from the leading edge (Fig. 6g). These results suggest that in Ptcd/+ heterozygote cells, Coro1A^{WT} can access the leading edge to regulate actin dynamics. In summary, the biochemical studies indicate that the highly conserved Glu26 residue in Coro1A is important for regulation of Arp2/3.

Coronin-1A is deficient in a T^{-} B^{+}NK^{+} SCID patient

With Coro1A point mutations causing severe T lymphopenia in both *Ptcd* and *Koy*, we asked whether mutations in CORO1A could also be responsible for human primary T cell immunodeficiency cases with undefined etiologies. Thus, we sequenced *CORO1A* in DNA from sixteen SCID patients lacking mutations in previously recognized T^{-}B^{+}NK^{+} SCID genes. While we failed to detect any *CORO1A* mutations in fifteen samples, we did identify a single patient with a two nucleotide deletion in exon 3, c.248 249delCT (Fig. 7a), resulting in a frameshift and premature stop codon (p.Pro83ArgfsX10) within the CORO1A beta-propeller domain. Consistent with a destabilizing truncation, immunoblot analysis of Epstein Barr virus-immortalized B lymphoid cell lines derived from the patient's peripheral blood showed an absence of CORO1A protein (Fig. 7b). When this patient was 13 mo. old, she was hospitalized with a severe post-vaccination varicella infection. She was later diagnosed as an atypical T^{-}B^{+}NK^{+} SCID patient and treated by allogeneic bone marrow transplantation; her father, but not mother or sister, was heterozygous for the *CORO1A* 2bp deletion (Fig. 7a).

To test for *CORO1A* gene copy loss in the patient, we performed genomic QPCR with non-overlapping primers spanning *CORO1A* introns 1 through exon 11 and observed ~2-fold deficiency in product compared to a healthy control (Fig. 7c). In contrast, *S1PR1* (human S1P$_1$ gene) on chromosome 1 and *CORO7* (CORONIN-7) located telomeric to *CORO1A* on chromosome 16p, did not differ from the QPCR signal in control cells. Taken together with recent reports of copy number variation in chromosome 16p11.2, where *CORO1A* is located 16–18, these data suggest that our patient, who inherited a 2bp paternal deletion in one allele of *CORO1A*, has a deletion of her other *CORO1A* allele.

DISCUSSION

Through a forward genetics approach, we have identified a unique *Coro1a* allele that allows us to establish a requirement for this actin-regulatory protein in T cell egress from thymus and lymph nodes. Two-photon microscopy reveals that Coro1A is needed for normal T cell motility within the lymph node and in vitro motility studies indicate a role in cell shape regulation. Moreover, this mutation reveals a site on Coro1A critical for Arp2/3 regulation and for the control of Coro1A distribution in the cell. Finally, we demonstrate that human CORO1A-deficiency can be associated with a peripheral T cell-deficiency of such severity to cause $T^{-}B^{+}NK^{+}$SCID.

The identification of a critical role for Coro1A in thymic and lymph node egress provides evidence that migration from these tissues depends on proper regulation of Arp2/3-mediated actin branching, most likely in response to S1P. mDia1, a member of the formin family of actin nucleating proteins that promote formation of unbranched actin filaments is also needed for thymic egress 19. Thus, both the formation of correctly branched as well as unbranched actin networks appears to be required for exit from this organ. The role of mDia1 in lymph node egress has not been assessed. The small G-proteins Rac and Cdc42 induce activation of the Wiskott-Aldrich syndrome protein (WASP)-Arp2/3 system and consistent with the studies here, the Rac activator DOCK2 is needed for lymph node egress 20. Although the role of DOCK2 in thymic egress has not been determined, given the need for Coro1A we anticipate DOCK2 will also be involved. Lymphocyte protrusions initiate diapedesis 21 and our findings suggest that Coro1A-dependent control of actin may play a critical role in the formation of protrusions during T cell egress.

The requirement for Arp2/3-mediated actin branching for T cell migration responses to chemoattractants has been supported by findings in DOCK2, WASP and WASP-interacting protein deficient cells 20,22,23 as well as Coro1A-deficient cells 6,7. Our results with *Ptcd* T cells add to these findings and suggest an important role for Coro1A-mediated Arp2/3 regulation in the control of T cell shape. A recent study argued that F-actin dynamics were unaltered in Coro1A-deficient T cells, although it did not examine cell migration in response to chemoattractants 8. The basis for these discrepant findings is unclear but it seems possible that the very poor survival of Coro1A-deficient naive T cells and their consequent depletion from T cell preparations relative to effector and/or memory T cells confounded some of the comparisons. In the present study we have been cautious to exclude both dead cells and effector or memory cells from our naive T cell analysis. Although *Ptcd* T cell migration was strongly reduced in vitro and within the lymph node, it was not absent and this might explain the continued ability of the *Ptcd* mouse thymus to organize into cortex and medulla3. The lack of marked defects in *Ptcd* and Coro1A-deficient B cells seems likely to be due to redundancy with other coronin family members and adds to other data establishing differences in requirements for B and T cell motility 19,24,25. Whether mutations in Coro1A or other actin regulatory genes cause defects in common lymphoid progenitors remains to be seen. While bone marrow chimera reconstitution efficiencies were similar between *Ptcd* and control donors, our studies have not formally addressed whether entry of early thymic precursors is impaired. It will be valuable in future studies to perform competition assays with mixed bone marrow chimeras to evaluate the proportion of *Ptcd*

derived cells in bone marrow and thymus. Leukocyte migration within lymphoid tissue has been described as phases of force-generating actin protrusions followed by myosin-dependent contractions 26 that aid the squeezing of the cell nucleus through three-dimensional matrices. In this regard it is notable that *Ptcd* T cells not only display large and dysmorphic protrusions but also fail to elongate their nuclei. Thus, Coro1A remodeling of the actin cytoskeleton may contribute to both protrusion and contraction during T cell migration through lymphoid tissues.

The mechanism by which coronins inhibit Arp2/3-mediated actin branching is complex and incompletely understood. Although several studies have shown coronins are able to directly bind Arp2/3 and possibly inhibit function prior to F-actin binding 27,28, recent work on Coro1B in fibroblasts suggests that it acts by displacing Arp2/3 from actin branch points29. We demonstrate the involvement of a Coro1A surface proximal to the predicted F-actin binding region13 as being involved in Arp2/3 regulation. Our findings highlight the importance of characterizing the highly conserved Glu26 containing surface of the type I coronin subfamily in future structure-function studies focusing on how an oligomeric coronin complex dislodges Arp2/3 from F-actin. The failure of Coro1A^{E26K} to localize normally to the leading edge of migrating cells identifies what may be another level of coronin regulation. Further studies will be needed to determine whether interactions with the cofilin phosphatase, slingshot5, or other still unknown coronin binding partners are altered by the mutation.

Coro1A-deficiency causes a severe defect in T cell survival but the basis for this effect is not yet resolved. While the *Ptcd* is an important allelic comparison that disconnects the survival and Ca^{2+} flux defects, the elevated phalloidin staining in Ptcd/− mature thymocytes also fails to support a simple correlation between survival and F-actin accumulation. The possibility that Coro1A directly impacts cell survival independent of effects on F-actin remains, and analysis of additional Coro1A mutations may yield new allelic insights. The continued ability of *Ptcd* thymocytes to maintain near normal total cellular F-actin despite the mislocalization of the Coro1A protein might be explained by ongoing association of low but sufficient amounts of Coro1A^{E26K} to achieve partial leading edge Arp2/3 regulation, or might reflect a corresponding increase in actin-debranching and depolymerization in the cell body. Alternatively, the *in vitro* assay for examining Arp2/3 and Coro1A colocalization may not accurately reflect how these proteins distribute *in vivo* in migrating thymocytes. The similar partial deficiencies in TCR-induced Ca^{2+} flux in Coro1A^{E26K} and *Coro1a*$^{-/-}$ T cells are in agreement with emerging evidence that an intact actin cytoskeleton is important for Ca^{2+} flux 30. But our finding that CD3-CD4 co-crosslinking led to equivalent Ca^{2+} flux in wild-type, Coro1A^{E26K} and *Coro1a*$^{-/-}$ thymocytes, along with a recent report6 that found normal proliferation of *Coro1a*$^{-/-}$ T cells stimulated by antigen-presenting cells, suggest that Coro1A may have a limited role in TCR signaling during cognate antigen encounters. We anticipate that single cell analysis of calcium store release and CRAC channel activity in *Ptcd* and Coro1A-deficient mature thymocytes and T cells, along with similar studies of T cells with other actin regulatory protein defects, will add to future understanding of how the actin cytoskeleton contributes to calcium signaling.

An important challenge with studies in mouse models is translation of the findings to humans. The identification of a patient with a peripheral T cell deficiency who lacks expression of Coro1A strongly suggests that Coro1A has similar functions in humans as in mice. While the human X-linked Wiskott Aldrich syndrome has long associated actin biology with haematopoietic cell dysfunction, the *CORO1A* deficient patient allows us to link regulation of the actin cytoskeleton with SCID 31. $T^{-}B^{+}NK^{+}$ SCID has previously been defined by mutations impairing TCR or IL-7R signaling 32. Other forms of SCID involve defects in purine metabolism, DNA recombination, or cytokine signaling 33. Mutations in these pathways result in apoptosis through purine toxicity, deficient cytokine signaling, or failure to rearrange a signaling competent antigen receptor. With *CORO1A* deficiency, we can also include apoptosis through actin dysregulation as a cause of SCID. A recent report classifying a *Coro1a*-null allele as an autoimmune-suppressing locus in mice 7 is consistent with Coro1A defects causing immunodeficiency. We predict that mutations in other hematopoeitic-specific actin-associated molecules will be found to cause SCID. Because the pericentromeric segment of human chromosome 16 containing *CORO1A* is prone to copy number variation 16–18, we also anticipate that additional cases of patients with reduced T cell function will involve *CORO1A* mutations.

METHODS

Mice, ENU-mutagenesis and bone marrow chimeras

C57BL/6 (B6) and B6-CD45.1 mice were obtained from Jackson Laboratories, National Cancer Institute, or a colony maintained at the University of California, San Francisco. UBC-GFP mice were purchased from Jackson Laboratories. Cataract Shionogi (CTS/Shi) mice were purchased from TGC (Tokyo, Japan). The *Ptcd* locus was backcrossed 6–10 generations onto B6 using SNP markers as described below. *Coro1a*$^{-/-}$ mice, which were backcrossed 10 generations with B6, were generated as described 6. Koyaanisqatsi (*Koy*) mice were identified in an ENU-mutagenesis screen performed as described 34 using B6 mice in a colony maintained at the Australian National University. Briefly, male B6 mice were treated with three doses, 1 wk apart, of 100 mg/kg *N*-ethyl-*N*-nitrosourea (Sigma) in 10% ethanol, citrate buffer (pH 5.0) to produce G0 mice. Following an 8 wk refractory period, these G0 males were mated with B6 females to generate G1 offspring. Two unrelated G1 mice were crossed producing G2 mice, which, were then intercrossed to yield G3 mice. Screening of these G3 mice by flow cytometry identified the *Koy* phenotype. All mice were housed in specific pathogen-free conditions; and all protocols were approved by the Institutional Animal Care and Use Committee of the University of California, San Francisco, or the Australian National University AEEC. Bone marrow chimeras were generated with $2–3 \times 10^6$ bone marrow cells from donor mice intravenously transplanted into lethally irradiated congenic hosts. Chimeras were given prophylactic antibiotic water and analyzed 8–12 weeks after transplantation.

Flow cytometry, intracellular stains and calcium flux measurements

S1P1 polyclonal antibody was previously described 35. Phalloidin-FITC was from Sigma. Indo-1 was from Invitrogen. Intracellular staining and Annexin-V staining kits were from BD Bioscience. JC-1 mitochondrial membrane potential staining kit was from Cayman Inc.

All other antibodies used for flow cytometry were obtained from BD Biosciences, Invitrogen, eBiosciences, or BioLegend. Calcium flux assays were adapted from previously described methods for thymocytes 14. Briefly, cells were loaded at 30 °C for 30 min with Indo-1 in the presence of biotinylated anti-CD3 (clone 2C11, BD), anti-CD8 FITC (clone 53-6.7, BD), and anti-CD4 Alexa647 (clone RM4-5, BD). Thymocytes were additionally stained with anti-CD62L PE (clone Mel14, BD) and splenocytes with anti-CD44 PE (clone IM7, BD). Cells were washed and kept on ice until analysis. For anti-CD4 co-crosslinking, cells were additionally pre-treated for 5 min with biotinylated anti-CD4 (clone RM4-4, BD). Cells were mixed with pre-warmed media containing propidium iodide for exclusion of dead cells and warmed to 37 °C. Baseline calcium levels (ratio of UV-short to long) were assessed for 30 sec prior to streptavidin (50 ug/mL; Pierce) crosslinking. All flow cytometry was performed on BD FACalibur or BD LSRII.

Purification of recombinant protein

Coronin recombinant protein was expressed and purified with a mammalian expression system as described previously for Coronin 1B 15. Purified protein was quantified from absorbance at 280 nm and the predicted extinction coefficients of 62910 $M^{-1}cm^{-1}$ (Coronin 1A) and 65890 $M^{-1}cm^{-1}$ (Coronin 1B).

Immunoprecipitation

Cells were washed twice with phosphate-buffered saline and lysed with a KCl buffer (20 mM HEPES, pH 7.0, 100 mM KCl, 0.5% Nonidet P-40, 1 mM EDTA, 1 mM phenylmethylsulfonyl fluoride, 10 μg/ml 1,10-phenanthroline, 10 μg/ml aprotinin, 10 μg/ml leupeptin, 10 mM sodium fluoride, and 2 mM sodium orthovanadate). Lysates were cleared at 13,000 × *g* for 5 min and incubated with 0.5 μg of primary antibody for 16 h at 4 °C, followed by the addition of 20 μl of 50% slurry of ImmunoPure-immobilized protein A/G beads (Pierce) and further incubation at 4 °C for an additional hour. The immune complexes were collected, washed with the KCl buffer three times, separated by SDS-PAGE, and transferred to a polyvinylidene difluoridemembrane (Bio-Rad) for immunoblotting.

Actin assembly assay

VCA-induced Arp2/3 nucleation reactions were performed as previously 15: recombinant Coronin and Arp2/3 (20 nM) were mixed in MKEI-50 Buffer and incubated at room temperature for 5 min; reactions were initiated by the simultaneous addition of 1.5 μM actin (5% pyrene labeled, primed with 1 mM EGTA and 0.1 mM $MgCl_2$ for 90 s) and 1 nM GST-VCA. The delay between mixing reactants and recording fluorescence was 15 seconds. Fluorescence was converted to the molar concentration of F-actin from the fluorescence of completely polymerized (24 hr post reaction) and unpolymerized actin, assuming a critical concentration of 0.1 μM.

Immunoblot

Lysates from mouse thymocytes and human EBV-immortalized cell lines were prepared in RIPA buffer (1% NP-40, 0.5% sodium deoxycholate, 0.1% SDS, 50mM Tris-pH8.0, 150mM NaCl, 0.02 NaN3), resolved (NuPage, Invitrogen) and transferred (XCell,

Invitrogen) to Immobilon-FL (Millipore), blocked and probed with LICOR buffer, and analyzed on an Odyssey Infrared Imager (LICOR). Anti-Coro1A was from Upstate; anti-actin from Sigma, and secondary IREDye antibodies were from Rockland.

Transwell migration

Transwell migration assays (5 micron; Corning) were performed with thymocytes or splenocytes collected in migration media (RPMI (Cellgro) supplemented with 10 mM HEPES (Cellgro), 100 U/mL penicillin-streptomycin (Cellgro), and 0.5% Fatty Acid Free BSA (Calbiochem)). For S1P migration, thymocytes were assayed immediately after isolation. For chemokine migration, thymocytes or RBC-lysed splenocytes were resensitized in migration media for 30 min at 37 °C. S1P (Sigma), human SDF-1a (Peprotech) and mouse CCL21 and CXCL13 (R&D Systems) were used at the concentrations indicated.

Adoptive cell transfers and treatments

Thymocytes were labeled with CFSE or CellTracker Orange CMTMR (Molecular Probes) as described 36. For adoptive transfer, mice were injected intravenously with ~1–3 × 10^7 cells in ~0.3 mL of media. For homing assays, mice were analyzed 1 h post-transfer. For peripheral egress assays, mice were analyzed 24 h post-transfer or treated intravenously with entry blocking antibodies for 20 h and analyzed after 44 h. Antibodies used for in vivo entry blockade were previously described 37.

Two-photon microscopy

Thymocytes from donor mice were isolated and labeled with CellTracker Orange CMTMR (Invitrogen-Molecular Probes) as described 38 and intravenously injected with thymocytes from UBC-GFP mice into B6 recipient mice. After 12–24 h, inguinal lymph nodes were isolated for two-photon microscopy, and axillary and brachial lymph nodes were isolated for flow cytometry. Flow cytometric analysis confirmed that >90% of CMTMR-positive cells in lymph nodes were mature single-positive thymocytes ($CD4^+CD8^-CD69^{lo}CD62L^{hi}$ or $CD4^-CD8^+$ $CD69^{lo}CD62L^{hi}$). Explants were prepared as described 39. Inguinal lymph nodes were perfused with RPMI (Cellgro) at 36–37 °C, aerated with 95% O_2/5% CO_2, and were imaged from the cortical side of the lymph node through the capsule. A ‘custom’ two-photon microscope system was used for imaging, with the 5-W MaiTai TiSapphire laser (Spectra-Physics) tuned at an 890 nm excitation wavelength. Images were captured with Video Savant software (IO Industries). For time-lapsed imaging, 30–36 planes spaced 3 um apart were collected every 20 s. Each *xy* plane spanned 240 um × 288 um at a resolution 0.6 um per pixel. Data were further processed with MetaMorph software (Molecular Devices). Imaris software (Bitplane AG) was used for three-dimensional volume rendering and cell tracking. Matlab software was further used to calculate cell velocities, turning angles, and displacement. Statistical significance was evaluated with a paired two-tailed Student’s *t*-test.

Genetic mapping, SNP analysis, human samples, and sequencing

CTS/Shi mice were crossed with B6 to generate an F1 generation. The *Ptcd* locus was mapped with mutant F2 progeny from F1 intercrosses, F1 backcrossed to nonparental CTS, or mutant F2 crossed with nonparental F1. Mice were phenotyped by flow cytometric

analysis of thymocyte subset frequencies. Genomic DNA was isolated from tails (Wizard Genomic Kit, Promega) and SNP reactions were performed with Amplifluor HT-kit (Chemicon, Millipore) on an ABI7300 (Applied Biosystems) according to manufacturer's instructions. Mapping SNPs were selected based on polymorphisms between B6 and BUB/J, a strain closely related to CTS/Shi. SNP primers were designed on the AssayArchitect website. Patients with SCID and their parents, if available, were enrolled with informed content in IRB-approved protocols to determine genotype and genotype/phenotype correlations. Blood samples were immortalized with Epstein-Barr Virus (EBV) to create B cell lines. Human genomic DNA was isolated from buccal swabs or EBV-immortalized lines with a Puregene kit (Gentra Systems). Genomic QPCR was performed on an ABI7300. Human and mouse *Coro1a* exons and surrounding splice regions were amplified by PCR from genomic DNA, resequenced, and analyzed on 4Peaks relative to reference human genomic and cDNA sequences NM_007074 and NM_007074.2, respectively. Primers are summarized in Supplementary Table 1 online.

Brightfield and immunofluorescenct microscopy

For fixed immunofluorescent imaging, 1–2 × 10^6 lymphocytes from peripheral and mesenteric lymph nodes were seeded on chambered coverslips (Lab-tek, Nunc) precoated with 10 ug/mL recombinant mouse ICAM1-Fc (R&D Systems), and allowed to settle and migrate in the presence of 1 ug/mL CCL21 (R&D Systems) for 1 h at 37 °C in RPMI (Cellgro) supplemented with 1% Fetal Calf Serum (Invitrogen), 10mM HEPES (Cellgro), and 100 U/mL penicillin-streptomycin. Cells were then fixed with 4% (wt/vol) paraformaldehyde (Sigma) and permeabilized with 0.5% Triton-X100 (Sigma) in PBS. Coverslips were then stained with a combination of the following: anti-Coronin-1A (rabbit polyclonal, Millipore/Upstate) or anti-p34Arc (rabbit polyclonal, Millipore/Upstate), FITC-conjugated phalloidin (Sigma), Alexa647-conjugated anti-CD4 (clone RM4-5, BD), Alexa647-conjugated anti-CD8 (clone 53-6.7, BD), biotinylated goat anti-rabbit (BD), streptavidin-Cy3 (Jackson Immuno), or DAPI (Molecular Probes). Z-stacks were captured on an Axiovert Z1 (Zeiss) and deconvoluted with Axiovision Software (Zeiss). For real-time imaging, 5 × 10^5 lymphocytes from peripheral and mesenteric lymph nodes were stained with PE-conjugated anti-CD19 (clone 1D3, BD) and Alexa647-conjugated anti-CD4 and anti-CD8 and seeded on ICAM-coated chambered coverslips with CCL21 as described above with the addition of 0.1% NuSieve GTG Low Melt Agarose (FMC BioProducts) and DAPI. Cells were maintained at 37 °C and 5% CO2 during 3–4 h of imaging in an environmentally-controlled stage on an Axiovert Z1. Each 5 min movie was generated with 10 s time-lapse intervals containing 6 brightfield 0.5 micron *z*-stacks. Following time-lapse, a fluorescence image was captured to identify live T cells. Movies and images were processed with Axiovision (Zeiss) and exported for annotation and splicing with AfterEffects (Adobe).

Supplementary Material

Refer to Web version on PubMed Central for supplementary material.

Acknowledgments

We'd like to thank the SCID patient and her family. We also thank M. Anderson, P. Beemiller, S. Cheung, G. Cinamon, M. Krummel, T. Phan, H. Phee, and A. Weiss for helpful discussions, and D. Schafer for helpful advice and reagents related to the pyrene actin assay. This work was supported by the UCSF Medical Scientist Training Program and a Genentech-Sandler Graduate Research Fellowship (L.R.S.), the US Immunodeficiency Network and Jeffrey Modell Foundation (J.M.P.), the Howard Hughes Medical Institute (J.G.C.), and grants from the National Institutes of Health (C.C.G., J.B. and J.G.C.).

References

1. Schwab SR, Cyster JG. Finding a way out: lymphocyte egress from lymphoid organs. Nat Immunol. 2007; 8:1295–1301. [PubMed: 18026082]
2. Ohtori H, Yoshida T, Inuta T. "Small eye and cataract," a new dominant mutation. Exp Animals. 1968; 17:91–96.
3. Yagi H, et al. Defect of thymocyte emigration in a T cell deficiency strain (CTS) of the mouse. J Immunol. 1996; 157:3412–3419. [PubMed: 8871639]
4. Ikegami H, Makino S, Harada M, Eisenbarth GS, Hattori M. The cataract Shionogi mouse, a sister strain of the non-obese diabetic mouse: similar class II but different class I gene products. Diabetologia. 1988; 31:254–258. [PubMed: 3133269]
5. Uetrecht AC, Bear JE. Coronins: the return of the crown. Trends Cell Biol. 2006; 16:421–426. [PubMed: 16806932]
6. Foger N, Rangell L, Danilenko DM, Chan AC. Requirement for coronin 1 in T lymphocyte trafficking and cellular homeostasis. Science. 2006; 313:839–842. [PubMed: 16902139]
7. Haraldsson MK, et al. The lupus-related Lmb3 locus contains a disease-suppressing Coronin-1A gene mutation. Immunity. 2008; 28:40–51. [PubMed: 18199416]
8. Mueller P, et al. Regulation of T cell survival through coronin-1-mediated generation of inositol-1,4,5-trisphosphate and calcium mobilization after T cell receptor triggering. Nat Immunol. 2008; 9:424–431. [PubMed: 18345003]
9. Kimura S, et al. Genetic control of peripheral T-cell deficiency in the cataract Shionogi (CTS) mouse linked to chromosome 7. Immunogenetics. 1998; 47:278–280. [PubMed: 9435347]
10. Ohotori H, Yoshida T, Inuta T. Small eye and cataract, a new dominant mutation in the mouse. Jikken Dobutsu. 1968; 17:91–96.
11. Nal B, et al. Coronin-1 expression in T lymphocytes: insights into protein function during T cell development and activation. Int Immunol. 2004; 16:231–240. [PubMed: 14734608]
12. Appleton BA, Wu P, Wiesmann C. The crystal structure of murine coronin-1: a regulator of actin cytoskeletal dynamics in lymphocytes. Structure. 2006; 14:87–96. [PubMed: 16407068]
13. Cai L, Makhov AM, Bear JE. F-actin binding is essential for coronin 1B function in vivo. J Cell Sci. 2007; 120:1779–1790. [PubMed: 17456547]
14. Maltzman JS, Kovoor L, Clements JL, Koretzky GA. Conditional deletion reveals a cell-autonomous requirement of SLP-76 for thymocyte selection. J Exp Med. 2005; 202:893–900. [PubMed: 16186188]
15. Cai L, Marshall TW, Uetrecht AC, Schafer DA, Bear JE. Coronin 1B coordinates Arp2/3 complex and cofilin activities at the leading edge. Cell. 2007; 128:915–929. [PubMed: 17350576]
16. Ghebranious N, Giampietro PF, Wesbrook FP, Rezkalla SH. A novel microdeletion at 16p11.2 harbors candidate genes for aortic valve development, seizure disorder, and mild mental retardation. Am J Med Genet A. 2007; 143:1462–1471. [PubMed: 17568417]
17. Weiss LA, et al. Association between microdeletion and microduplication at 16p11.2 and autism. N Engl J Med. 2008; 358:667–675. [PubMed: 18184952]
18. Kumar RA, et al. Recurrent 16p11.2 microdeletions in autism. Hum Mol Genet. 2008; 17:628–638. [PubMed: 18156158]
19. Sakata D, et al. Impaired T lymphocyte trafficking in mice deficient in an actin-nucleating protein, mDia1. J Exp Med. 2007; 204:2031–2038. [PubMed: 17682067]

20. Nombela-Arrieta C, et al. A central role for DOCK2 during interstitial lymphocyte motility and sphingosine-1-phosphate-mediated egress. J Exp Med. 2007; 204:497–510. [PubMed: 17325199]
21. Carman CV, et al. Transcellular diapedesis is initiated by invasive podosomes. Immunity. 2007; 26:784–797. [PubMed: 17570692]
22. Gallego MD, et al. WIP and WASP play complementary roles in T cell homing and chemotaxis to SDF-1alpha. Int Immunol. 2006; 18:221–232. [PubMed: 16141245]
23. Snapper SB, et al. WASP deficiency leads to global defects of directed leukocyte migration in vitro and in vivo. J Leukoc Biol. 2005; 77:993–998. [PubMed: 15774550]
24. Reif K, et al. Cutting edge: differential roles for phosphoinositide 3-kinases, p110gamma and p110delta, in lymphocyte chemotaxis and homing. J Immunol. 2004; 173:2236–2240. [PubMed: 15294934]
25. Nombela-Arrieta C, et al. Differential requirements for DOCK2 and phosphoinositide-3-kinase gamma during T and B lymphocyte homing. Immunity. 2004; 21:429–441. [PubMed: 15357953]
26. Lammermann T, et al. Rapid leukocyte migration by integrin-independent flowing and squeezing. Nature. 2008; 453:51–55. [PubMed: 18451854]
27. Humphries CL, et al. Direct regulation of Arp2/3 complex activity and function by the actin binding protein coronin. J Cell Biol. 2002; 159:993–1004. [PubMed: 12499356]
28. Rodal AA, et al. Conformational changes in the Arp2/3 complex leading to actin nucleation. Nat Struct Mol Biol. 2005; 12:26–31. [PubMed: 15592479]
29. Cai L, Makhov AM, Schafer DA, Bear JE. Coronin 1B antagonizes Cortactin and remodels Arp2/3-containing actin branches in lamellipodia. Cell. 2008 in press.
30. Gallo EM, Cante-Barrett K, Crabtree GR. Lymphocyte calcium signaling from membrane to nucleus. Nat Immunol. 2006; 7:25–32. [PubMed: 16357855]
31. Puck JM, Candotti F. Lessons from the Wiskott-Aldrich syndrome. N Engl J Med. 2006; 355:1759–1761. [PubMed: 17065636]
32. Fischer A. Human primary immunodeficiency diseases. Immunity. 2007; 27:835–845. [PubMed: 18093537]
33. Buckley RH. The multiple causes of human SCID. J Clin Invest. 2004; 114:1409–1411. [PubMed: 15545990]
34. Nelms KA, Goodnow CC. Genome-wide ENU mutagenesis to reveal immune regulators. Immunity. 2001; 15:409–418. [PubMed: 11567631]
35. Lo CG, Xu Y, Proia RL, Cyster JG. Cyclical modulation of sphingosine-1-phosphate receptor 1 surface expression during lymphocyte recirculation and relationship to lymphoid organ transit. J Exp Med. 2005; 201:291–301. [PubMed: 15657295]
36. Shiow LR, et al. CD69 acts downstream of interferon-alpha/beta to inhibit S1P1 and lymphocyte egress from lymphoid organs. Nature. 2006; 440:540–544. [PubMed: 16525420]
37. Pham TH, Okada T, Matloubian M, Lo CG, Cyster JG. S1P1 receptor signaling overrides retention mediated by G alpha i-coupled receptors to promote T cell egress. Immunity. 2008; 28:122–133. [PubMed: 18164221]
38. Allen CD, Okada T, Tang HL, Cyster JG. Imaging of germinal center selection events during affinity maturation. Science. 2007; 315:528–531. [PubMed: 17185562]
39. Okada T, et al. Antigen-engaged B cells undergo chemotaxis toward the T zone and form motile conjugates with helper T cells. PLoS Biol. 2005; 3:e150. [PubMed: 15857154]

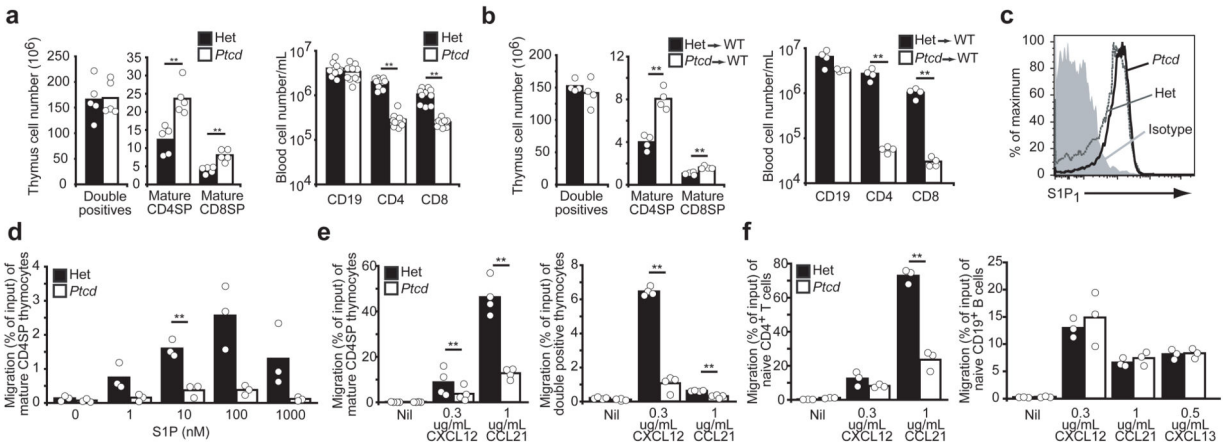

Figure 1. Peripheral T cell deficiency (*Ptcd*) is an intrinsic T cell migration. (a, b)

Thymocyte and peripheral blood lymphocyte subsets from B6 *Ptcd* (white) and control mice (black) (**a**), or wild-type mice reconstituted with *Ptcd* (white) or control (black) bone marrow (**b**). Columns represent means and circles represent individual mice. **(c)** Flow cytometric analysis of $S1P_1$ on mature CD4SP thymocytes from *Ptcd* (solid) and control (dotted) mice; isotype control in filled histogram. Representative of three experiments. **(d–f)** Transwell migration of *Ptcd* (white) or control (black) mature CD4SP thymocytes to S1P in (**d**), thymocytes to indicated chemokines in (**e**), or splenic naive $CD4^+$ T cell or $CD19^+$ B cells to indicated chemokines in (**f**), are shown as percentage of input that migrated. Columns represent means and circles represent individual mice pooled from three or four experiments. ** $P < 0.05$

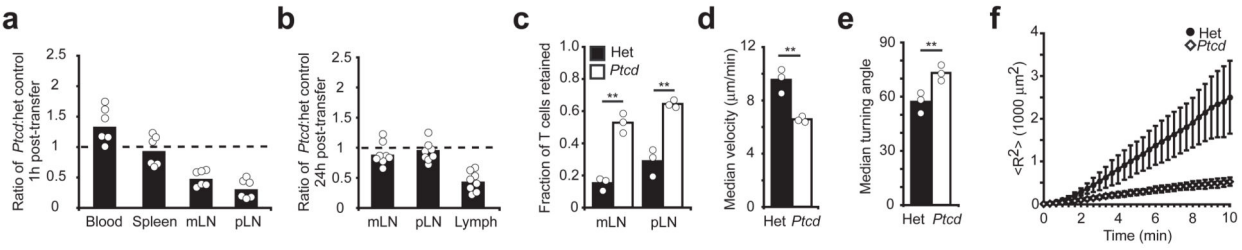

Figure 2. *Ptcd* T cells are defective in lymph node trafficking

(a,b) Homing to lymph nodes 1 h (**a**) and egress into lymph 24 h (**b**) following adoptive co-transfer of *Ptcd* (Ptcd/Ptcd) and control (Ptcd/+) thymocytes represented graphically as the ratio of *Ptcd* to control cells normalized to the injection *Ptcd*: control ratio. To achieve ~1:1 lymph node ratio at 24 h, initial injections were performed at a 3:1 ratio. Columns represent means and circles represent individual mice pooled from three experiments. **(c)** Fraction of *Ptcd* or control cells retained in the mesenteric (mLN) or peripheral (pLN) lymph nodes 20 h following treatment with integrin neutralizing antibody. Columns represent means and circles represent average values from independent experiments conducted with four mice each. **(d–f)** Time-lapse two-photon microscopy of explanted lymph nodes containing *Ptcd* and heterozygote control cells. Data representative of three independent experiments with at least 40 tracks analyzed in each. Mean velocities (**d**) and turning angles (**e**) of *Ptcd* cells (white) or control cells (black). Columns represent means and circles represent individual experiments. **(f)** Average of displacement squared $<R^2>$ over time of *Ptcd* (open diamond) or control cells (black circle). Symbols represent means and bars represent standard deviation. Het, control cells (Ptcd/+). ** $P <$ value<0.05

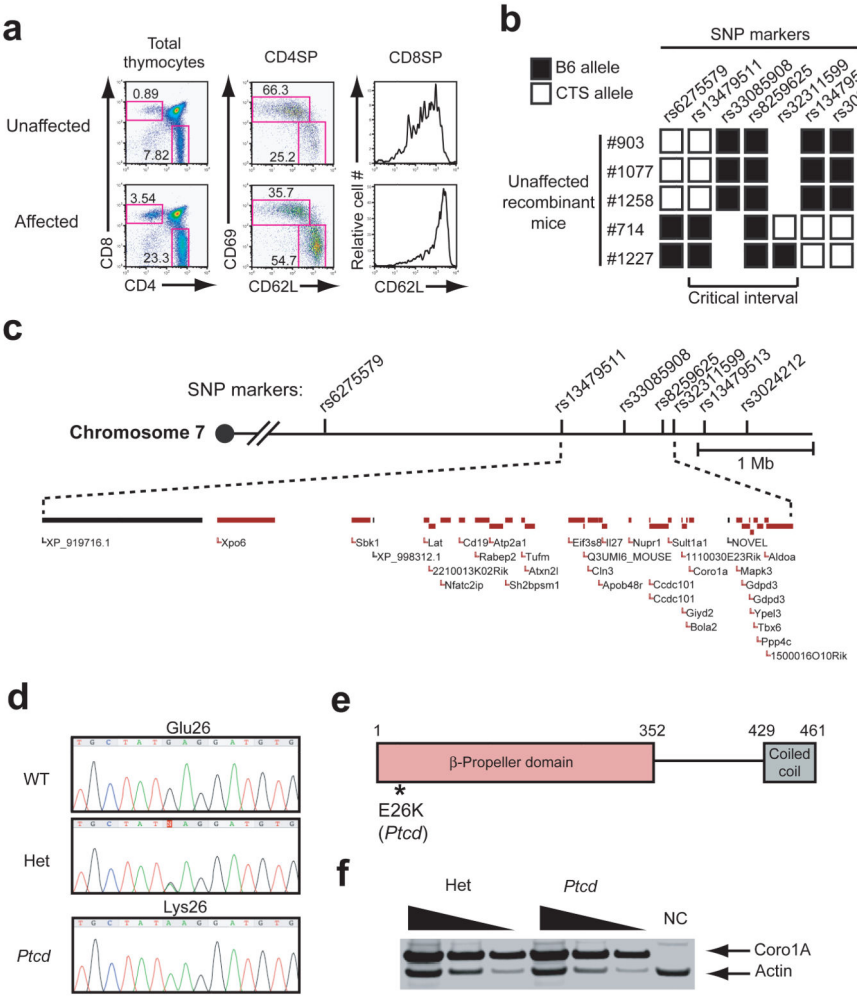

Figure 3. Coro1A is mutated at the *Ptcd* locus. (a)
Representative flow cytometric analysis of *Ptcd* mapping cross progeny used to phenotype affected or unaffected mice. Phenotype scored on single-positive frequencies, fraction of $CD62L^{hi}$ $CD69^{lo}$ CD4SP, and expression level of CD62L in CD8SP. **(b)** *Ptcd* critical interval defined by SNP markers polymorphic between B6 (black) and CTS (white) within indicated recombinant mice. **(c)** Schematic of open reading frames within the 950kb *Ptcd* critical interval (adapted from Ensembl). **(d)** Dideoxy sequence tracings of DNA from *Ptcd* and heterozygous mice revealing a 76G->A mutation causing a protein E26K substitution. DNA from the related NOD mouse strain was used as an additional control. **(e)** Schematic of Coro1A structure with *Ptcd* point mutation indicated. **(f)** Immunoblot analysis of total thymocytes from *Ptcd* and control mice for Coro1A and actin. Samples loaded in threefold dilutions. NC, negative control (*Coro1a*$^{-/-}$). Respresentative of three experiments.

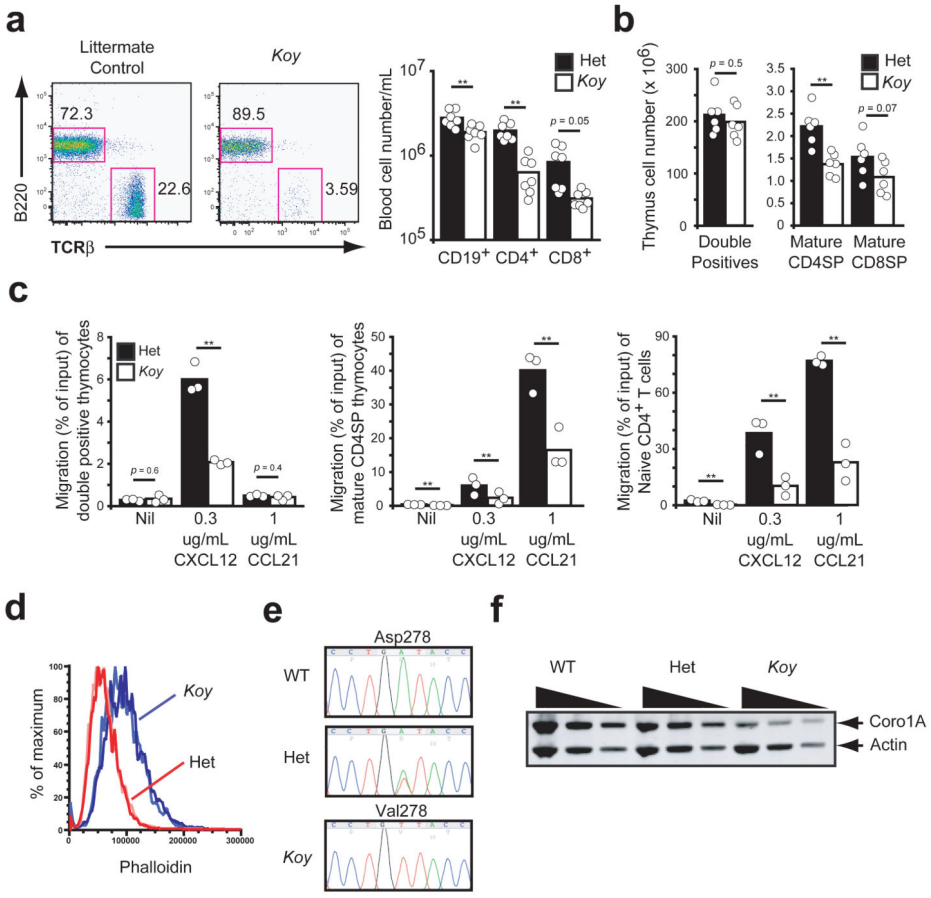

Figure 4. ENU-mutant *Koyaanisquatsi* is a Coro1A hypomorph

(a) Flow cytometric analysis from peripheral blood of *Koy* and littermate control mice demonstrated deficiency of TCRαβ$^+$ T lymphocytes (left). Lymphocytes subsets in peripheral blood of *Koy* (white) and control (black) mice (right). Columns represent means and circles represent individual mice. **(b)** Flow cytometric analysis of thymocyte subsets from *Koy* (white) and control (black). Columns represent means and circles represent individual mice. **(c)** Transwell migration of *Koy* (white) or control (black) double positive thymocytes, mature CD4SP thymocytes or splenic naive CD4$^+$ T cell to indicated chemokines are shown as percentage of input that migrated. Columns represent means and circles represent individual mice pooled from three experiments. **(d)** Flow cytometric analysis of phalloidin staining in mature CD4SP thymocytes from *Koy* (blue lines) and control mice (red lines). Each line is an individual mouse. Representative of at least three independent experiments. **(e)** Dideoxy sequence tracings from genomic tail DNA of *Koy* and control mice. **(f)** Immunoblot analysis from *Koy* and control mice as described in Fig. 3f. ** $P < 0.05$

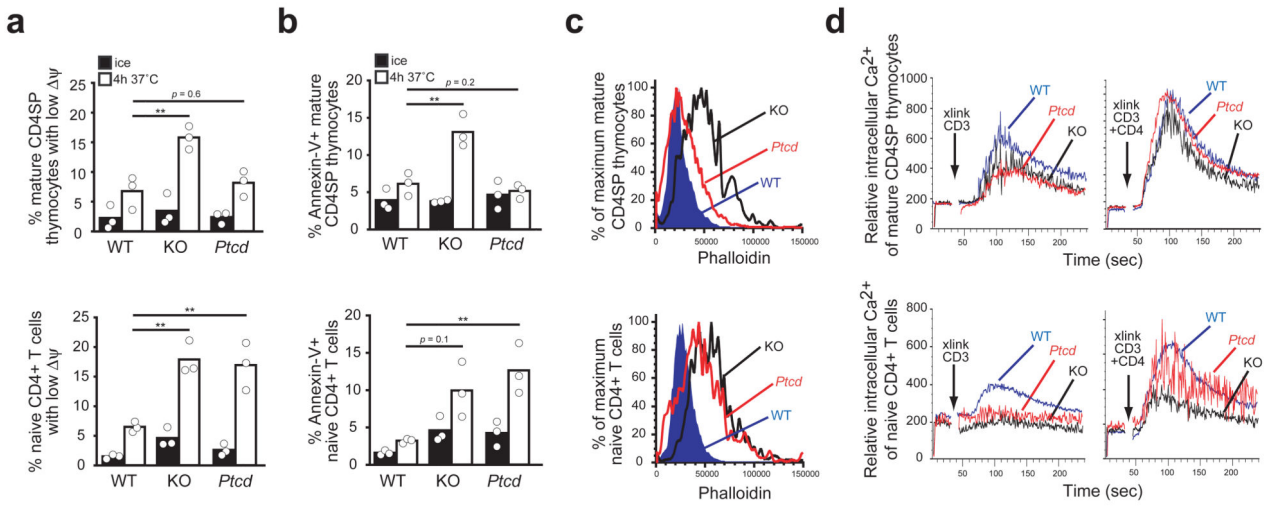

Figure 5. Allelic comparison of survival with F-actin accumulation and Ca^{2+} flux. (a,b) Apoptosis assessment by loss of mitochondrial membrane potential (**a**) or annexin-V staining (**b**) of mature CD4SP thymocytes (top) or naïve $CD4^+$ T cells (bottom) from wild-type, *Coro1a* 'knockout' and *Ptcd* mice following 4h incubation on ice (black) or at 37 °C (white). Pooled from three independent experiments. ** $P < 0.05$ **(c)** Flow cytometric analysis of phalloidin binding in mature CD4SP thymocytes (top) or naïve $CD4^+$ T cells (bottom) from wild-type, *Coro1a* knockout and *Ptcd* mice. Representative of at least three experiments. **(d)** Measurement of intracellular Ca^{2+} in mature CD4SP thymocytes (top) or naïve $CD4^+$ T cells (bottom) from wild-type, *Coro1a* knockout and *Ptcd* mice; prebound antibodies to CD3 or to CD3 and CD4 were crosslinked by addition of streptavidin at the time indicated. Dead and dying cells were excluded with propidium iodide staining. Representative of three experiments.

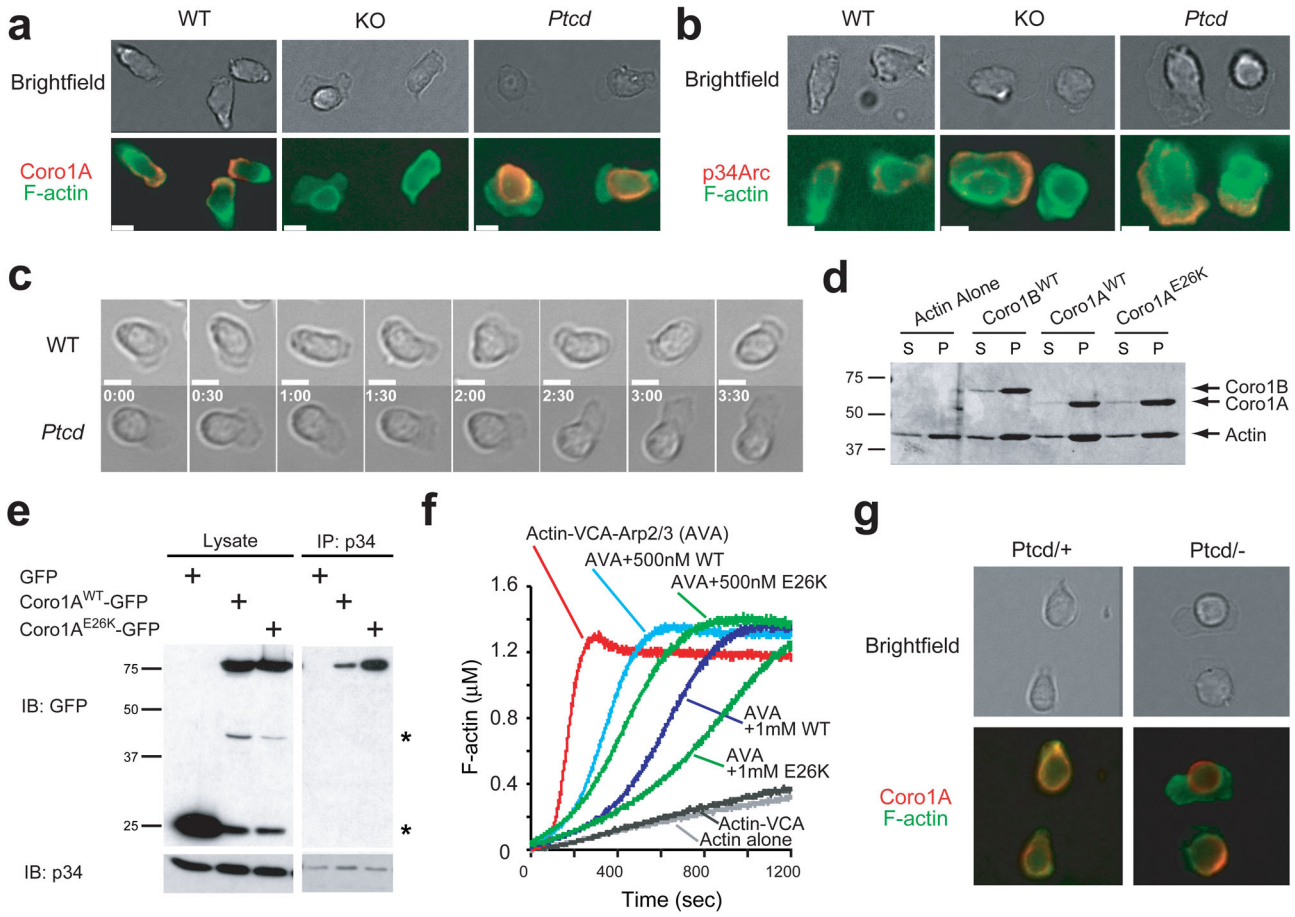

Figure 6. E26K mutation alters Coro1A cellular distribution and regulation of Arp2/3. (a–c) Immunofluorescent microscopy of T cells migrating on ICAM-coated coverslips in 1 ug/mL CCL21. Cells were stained for F-actin and (**a**) Coro1A or (**b**) Arp2/3 subunit p34 (**b**); and still images from brightfield time-lapse microscopy (**c**). White bar indicates 5 microns. Time stamp reflects min:sec. Data are representative of three experiments. **(d)** Co-sedimentation assay of indicated purified coronins and F-actin. S, supernatent. P, pellet. **(e)** Lysates from HEK293FT cells expressing indicated constructs were immunoprecipitated with anti-p34 and blotted with indicated antibodies. *GFP degradation bands. **(f)** Arp2/3-induced actin polymerization assay with indicated concentrations of purified coronins. WT, wild-type coronin. E26K, mutant coronin. AVA, standard mixture of actin, VCA and Arp2/3 complex **(g)** T cells from Ptcd/+ and Ptcd/− stained as in **a**.

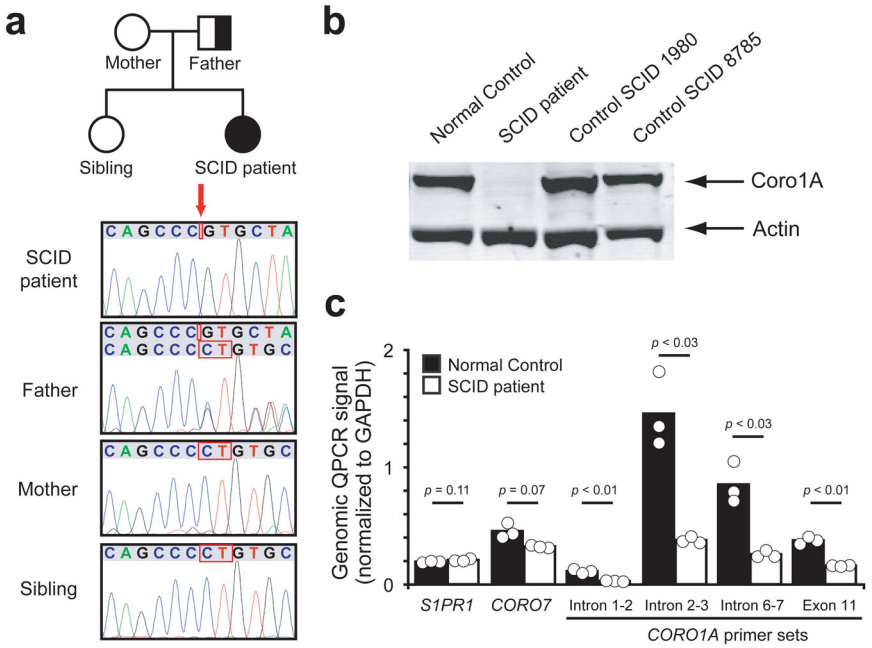

Figure 7. CORONIN-1A is deficient in a $T^{-}B^{+}NK^{+}$ SCID patient. (a)

Family pedigree and dideoxy sequence tracings from the patient and family members, with a red arrow (and empty red rectangle) indicating the location of c.248delCT in the patient that is heterozygous in the father and leads to a premature truncation after 10 missense codons. The father's sequence tracing is annotated to show both the mutated (top) and normal (bottom) copies. The CT nucleotides that are missing in the patient and in the father's mutated allele are boxed in the father's unmutated allele and in the sequence tracings obtained for the mother and sibling. **(b)** Immunoblot analysis for CORO1A and actin from EBV-transformed B cell lines derived from indicated subjects. Representative of three experiments. **(c)** Genomic QPCR signals from indicated primer sets of *S1PR1*, *CORO7* and *CORO1A* from buccal swab DNA of the SCID patient and normal control. Column represents mean and circles represent separate PCR reactions.